J. Fluid Mech. (1987), *vol.* 179, *pp.* 179–200
Printed in Great Britain

Axisymmetric vortex breakdown with and without temperature effects in a container with a rotating lid

By HANS J. LUGT

David W. Taylor Naval Ship Research and Development Center, Bethesda, MD 20084, USA

AND MICHEL ABBOUD†

Institut für Strömungslehre und Strömungsmaschinen, Universität Karlsruhe, 7500 Karlsruhe, West Germany

(Received 26 February 1986 and in revised form 15 October 1986)

A flow circulation in a closed circular-cylindrical container is produced by a rotating lid. After a transient phase from an initial state at rest a steady-flow situation is reached for a certain parameter range. In a subspace of this parameter range an undulating meridional flow occurs that may exhibit at the axis of rotation one or several separation bubbles which are interpreted as vortex breakdown. Numerical calculations on the basis of the Navier–Stokes equations for incompressible homogeneous and Boussinesq fluids enable the study of the influence of various flow parameters on the properties of these separation bubbles. The parameters varied are the Reynolds, Prandtl, Rayleigh, and Eckert numbers together with the ratio of height to radius of the container. The numerical results are in good agreement with experiments performed by Vogel, Ronnenberg, and Escudier. The stability of the fluid motions in these experiments with respect to non-axisymmetric disturbances strongly suggests that the corresponding axisymmetric solutions of the Navier–Stokes equations are stable configurations.

1. Background

A closed circular-cylindrical container with a lid is completely filled with a Newtonian fluid. Flow circulation is produced by the suddenly started constant rotation of the lid. After a transient period a steady-state fluid motion may be reached. Depending on the geometric and physical parameters involved, monotonic (that is, convex only, as seen from the boundaries) or undulating meridional streamline patterns develop. In the undulating fluid-flow mode axial stagnation points with a closed stream surface can occur (figure 1). This 'separation bubble' is interpreted as axisymmetric vortex breakdown in distinction to non-axisymmetric spiral vortex breakdown. Both types of vortex breakdown have been observed in pipes and chambers with swirling flows, in vortex filaments behind wing tips, and in atmospheric columnar vortices. Practical applications range from vortex control on modern aircraft to mixing in combustion chambers and to chemical reactions in swirling flows. The separation bubble, in particular, may serve as a liquid container which restricts or delays the mixing of the bubble fluid with its environment.

† Now at the Institut A für Mechanik, Universität Stuttgart, Pfaffenwaldring 9, 7000 Stuttgart 80, West Germany.

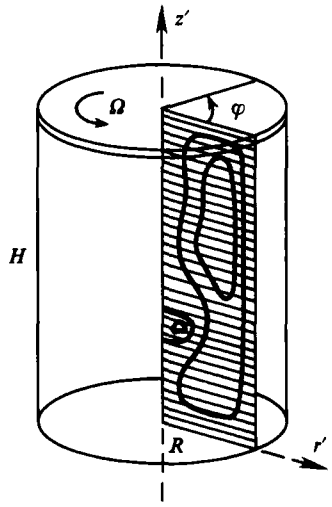

FIGURE 1. Container with a rotating lid. The meridional circulation with separation bubble is indicated by the shaded half-plane.

The literature on vortex breakdown is extensive. Some recent reviews are by Leibovich (1978), Escudier & Zehnder (1982), Wedemeyer (1982), and Leibovich (1984). The following discussion of previous work is therefore confined to vortex breakdown in a container, the specific subject of this paper.

The earliest reference to a phenomenon in a container that looks like axisymmetric vortex breakdown in the form of an open bubble (as interpreted by Maxworthy 1972) goes back to Wilcke in 1780. A bubble-like phenomenon was observed by Vettin (1857) in a rotating container. By local heating he created columnar vortices in which he observed the periodic appearance of a vortex ring. Vettin explained this phenomenon as being generated by the sucking of air into the low-pressure axis region at the top of the vortex. It is interesting that Wegener (1917, of continental-drift fame) related Vettin's separation bubble to a closed bubble of 'onion' shape which was clearly observed by Michaud in 1780 in waterspouts. More recently Maxworthy (see Bretherton, Carrier & Longuet-Higgins 1966) produced such a phenomenon, closely related to the container flow, between a stationary horizontal plate and a parallel plate above rotating in its own plane. Systematic experiments with container flow proper started with Vogel (1968) who was inspired at that time by the current lively debate on vortex breakdown (private communication). Vogel's motivation is particularly noteworthy since interpretation of the separation bubble in the container flow as a vortex-breakdown phenomenon was later questioned. (In some recent studies as, for instance, in those by Wedemeyer 1982 and Leibovich 1984, doubts expressed earlier were weakened somewhat by statements such as '...reversed flow regimes that resemble vortex breakdown'). Vogel's experiments were continued by Ronnenberg (1977) and Escudier (1984). They established the occurrence of steady separation bubbles in the parameter space (Reynolds number, ratio of height to radius of the container) as displayed in figure 2. Numerical calculations by Lugt & Haussling (1971, 1973) revealed the existence of transient separation bubbles outside the parameter range for which steady separation bubbles could exist. Later calculations within the parameter range (Lugt & Haussling 1982) confirmed the experimental results for steady-state bubbles by Vogel (1968), Ronnenberg (1977), and

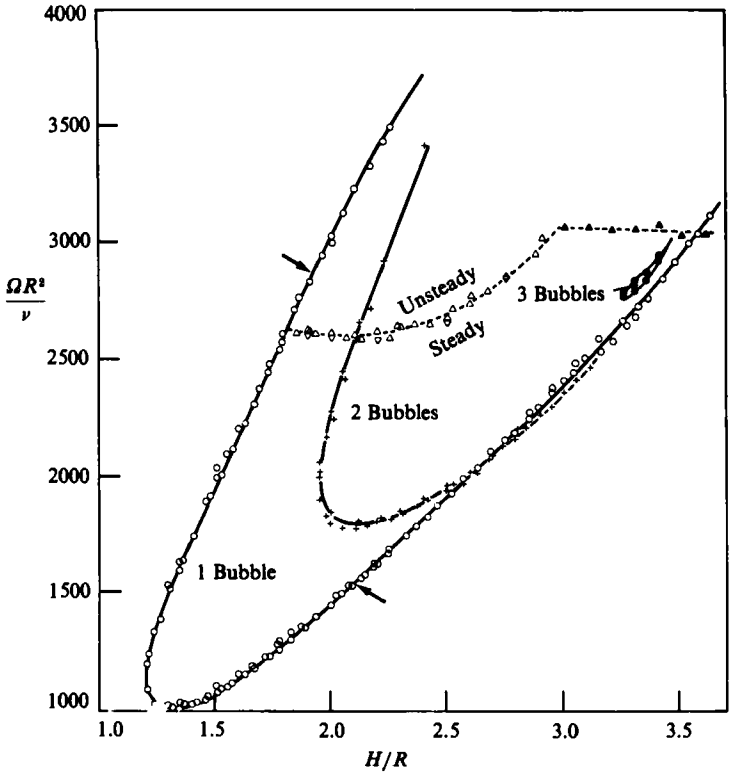

FIGURE 2. Boundaries for single, double, and triple separation bubbles and the boundary between oscillating and steady flows. The arrows designate the range of Vogel's experiments (after Escudier 1984).

Escudier (1984). Numerical calculations for the same flow problem at Reynolds numbers below the minimum values required for separation bubbles were performed by Dorfman & Romanenko (1966), Pao (1970, 1972), and Bertelà & Gori (1982). In all these papers the full Navier–Stokes equations were used but with the restriction of axisymmetry. This assumption precludes non-axisymmetric instability. Numerical results with temperature effects in a Boussinesq fluid outside the range where bubbles appear were published by Bertelà (1979). Studies with truncated Navier–Stokes equations were summarized by Grohne (1956).

The wavy nature of the meridional flow in figure 1 (and of the azimuthal velocity component) suggests that more than one bubble may occur. In fact, Sarpkaya (1971) observed in experiments up to three bubbles occurring simultaneously in a swirling pipe flow, and Grabowski & Berger (1976) found two bubbles in numerical computations for the same problem. Escudier (1984) determined systematically the occurrence of one, two, and three bubbles in the container flow and devised a diagram for the various modes (figure 2).

The purpose of this paper is to study numerically the development and occurrence of more than one bubble in detail, to confirm the close agreement between numerical computations and experiments especially with regard to stability arguments, and to inquire about the influence of temperature fields on the properties of those bubbles.

2. Statement of the problem

The circular-cylindrical container with radius R and height H is filled with either an incompressible homogeneous Newtonian fluid or a fluid under the restriction of the Boussinesq approximation. Both fluids have a constant dynamic viscosity μ, specific heat c_p, and thermal conductivity λ. The density of the incompressible homogeneous fluid has the same constant value everywhere, whereas the Boussinesq fluid has the density $\rho = \rho_0(1+\alpha\vartheta')$, where $\vartheta' = T_0' - T'$, T' is the temperature, and α is the thermal expansion coefficient. The subscript 0 denotes the state at the bottom of the container. The lid rotates with constant angular velocity Ω, and there is no gap between the container wall and the edge of the lid (figure 1).

Prior to time $t' = 0$ the fluid is at rest with the temperature T_1'. At $t' = 0$ the lid starts abruptly to rotate with $\Omega = \text{const.}$ and the bottom temperature changes to T_0'. As a result, meridional and azimuthal circulations develop that are considered laminar and axisymmetric, assumptions that are regarded as valid in this study. A gravitational force with constant g acts parallel to the axis of rotation. A heat flux takes place between the bottom and the lid. The sidewall is insulated.

For this problem the Navier–Stokes equations, the equation of continuity, and the energy equation for axisymmetric motion assume, in cylindrical polar coordinates r', φ, z' with corresponding velocity components u', v', w', the form

$$u'_{t'} + u'u'_{r'} + w'u'_{z'} - \frac{v'^2}{r'} = -\frac{1}{\rho_0}p'_{r'} + \nu\left[u'_{r'r'} + \left(\frac{u'}{r'}\right)_{r'} + u'_{z'z'}\right], \tag{1}$$

$$v'_{t'} + u'v'_{r'} + w'v'_{z'} + \frac{u'v'}{r'} = \nu\left[v'_{r'r'} + \left(\frac{v'}{r'}\right)_{r'} + v'_{z'z'}\right], \tag{2}$$

$$w'_{t'} + u'w'_{r'} + w'w'_{z'} = -\frac{1}{\rho_0}p'_{z'} - \alpha g\vartheta' + \nu\left[w'_{r'r'} + \frac{w'_{r'}}{r'} + w'_{z'z'}\right], \tag{3}$$

$$u'_{r'} + \frac{u'}{r'} + w'_{z'} = 0, \tag{4}$$

$$T'_{t'} + u'T'_{r'} + w'T'_{z'} = \frac{\lambda}{\rho_0 c_p}\left[T'_{r'r'} + \frac{1}{r'}T'_{r'} + T'_{z'z'}\right] + \frac{\mu}{\rho_0 c_p}\Phi, \tag{5}$$

with the dissipation function

$$\Phi = 2\left(u'^2_{r'} + \frac{u'^2}{r'^2} + w'^2_{z'}\right) + v'^2_{z'} + (w'_{r'} + u'_{z'})^2 + \left(v'_{r'} - \frac{v'}{r'}\right)^2, \tag{6}$$

where p' is the pressure and ν the constant kinematic viscosity μ/ρ_0. The set of equations (1)–(6) is valid for both incompressible homogeneous fluids when $\alpha = 0$ and Boussinesq fluids when $\alpha > 0$. The inclusion of dissipation is understood within the framework of the 'extended' Boussinesq approximation (Gray & Giorgini 1976). The adiabatic lapse rate is neglected in this study.

The initial and boundary conditions are

$$\left.\begin{array}{llllll}
t' < 0: & & u' = 0, & v' = 0, & w' = 0, & T' = T_1'; \\
t' \geqslant 0: & & & & & \\
z' = 0, & 0 \leqslant r' \leqslant R: & u' = 0, & v' = 0, & w' = 0, & T' = T_0'; \\
z' = H, & 0 \leqslant r' \leqslant R: & u' = 0, & v' = -\Omega r', & w' = 0, & T' = T_1'; \\
r' = R, & 0 \leqslant z' < H: & u' = 0, & v' = 0, & w' = 0, & \partial T'/\partial r' = 0; \\
r' = 0, & 0 \leqslant z' \leqslant H: & u' = 0, & v' = 0, & \partial w'/\partial r' = 0, & \partial T'/\partial r' = 0.
\end{array}\right\} \tag{7}$$

It is convenient to introduce the following dimensionless variables:

$$\left.\begin{gathered} t' = \frac{t}{\Omega}, \quad r' = Rr, \quad z' = Hz, \quad (u', v') = \Omega R(u, v), \quad w' = \Omega H w, \\ T' = (T_0' - T_1')\,T, \quad \vartheta = T - T_1, \end{gathered}\right\} \tag{8}$$

and the characteristic parameters

$$\left.\begin{aligned} \delta &= \frac{H}{R}, \\ Re &= \frac{\Omega R^2}{\nu} \quad \text{Reynolds number}, \\ Ra &= \frac{\delta^2 \alpha g (T_0' - T_1')}{\Omega^2 H} \quad \text{Rayleigh number}, \\ Pr &= \frac{\rho_0 c_p \nu}{\lambda} \quad \text{Prandtl number}, \\ Ec &= \frac{\Omega^2 R^2}{c_p (T_0' - T_1')} \quad \text{Eckert number}. \end{aligned}\right\} \tag{9}$$

The axisymmetry of the motion permits the stream function–vorticity formulation of the meridional flow. ψ denotes the dimensionless stream function and ζ the azimuthal component of the dimensionless vorticity vector

$$u = \frac{1}{r}\psi_z, \quad w = -\frac{1}{r}\psi_r, \tag{10}$$

$$\zeta = u_z - \delta^2 w_r, \tag{11}$$

Then, the initial-boundary-value problem to be solved is

$$\zeta_t + (u\zeta)_r + (w\zeta)_z - \left(\frac{v^2}{r}\right)_z = -Ra\,\vartheta_r + \frac{1}{Re}\left(\zeta_{rr} + \frac{1}{r}\zeta_r - \frac{1}{r^2}\zeta + \frac{1}{\delta^2}\zeta_{zz}\right), \tag{12}$$

$$v_t + (uv)_r + (wv)_z + 2\frac{uv}{r} = \frac{1}{Re}\left(v_{rr} + \frac{1}{r}v_r - \frac{v}{r^2} + \frac{1}{\delta^2}v_{zz}\right), \tag{13}$$

$$\delta^2\left(\psi_{rr} - \frac{1}{r}\psi_r\right) + \psi_{zz} = r\zeta, \tag{14}$$

$$\begin{aligned} \vartheta_t + u\vartheta_r + w\vartheta_z = {} & \frac{1}{Re\,Pr}\left(\vartheta_{rr} + \frac{1}{r}\vartheta_r + \frac{1}{\delta^2}\vartheta_{zz}\right) \\ & + \frac{Ec}{Re}\left[2\left(u_r^2 + \frac{u^2}{r^2} + w_z^2\right) + \left(v_r - \frac{v}{r}\right)^2 + \frac{1}{\delta^2}v_z^2 + \left(\frac{1}{\delta}u_z + \delta w_r\right)^2\right], \end{aligned} \tag{15}$$

with the boundary conditions for $t \geqslant 0$:

$$\left.\begin{aligned} z = 0, \quad 0 \leqslant r \leqslant 1: \quad & \psi = 0, \quad \psi_z = 0, \quad v = 0, \quad \vartheta = 1, \\ z = 1, \quad 0 \leqslant r \leqslant 1: \quad & \psi = 0, \quad \psi_z = 0, \quad v = -r, \quad \vartheta = 0, \\ r = 1, \quad 0 \leqslant z < 1: \quad & \psi = 0, \quad \psi_r = 0, \quad v = 0, \quad \partial\vartheta/\partial r = 0, \\ r = 0, \quad 0 \leqslant z \leqslant 1: \quad & \psi = 0, \quad \zeta = 0, \quad v = 0, \quad \partial\vartheta/\partial r = 0. \end{aligned}\right\} \tag{16}$$

At $z' = H, r' = R$ a singularity in the flow field occurs since there is no gap between container wall and edge of the lid. According to Lugt & Haussling (1971) this

singularity has the form $\lim_{r\to 1}(\partial v/\partial z) \sim (1-r)^{-1}$ and precludes the calculation of the torque coefficient of the lid. This situation was investigated by Schmieden (1928) for $Re = 0$, when no meridional circulation exists, with the width of the gap as a parameter, and on a 'heuristic basis' by Vogel (1968). Some researchers (Pao 1972; Bertelà & Gori 1982), nevertheless, claim to be able to approximate the torque coefficient by excluding the area about the singularity. This approach is considered by the authors to be not correct in principle.

For the calculation of the flow field, however, the singularity is of no consequence, since its influence is confined to its immediate neighbourhood.

3. Numerical integration

The initial-boundary-value problem defined by (12)–(16) is solved by using a straightforward finite-difference scheme. This scheme is essentially the same as that described by Lugt & Haussling (1973), except for the addition of the energy equation (15) and the accompanying initial boundary conditions.

After a stretching procedure to include variable grid sizes in the domain of integration, the linear operators of (12), (13), and (15) are replaced by the Dufort–Frankel approximation. The nonlinear operators are expressed by central-difference schemes. The Poisson equation (14) is solved by the Thomas algorithm along lines of constant r, a modified Gauss elimination process. A one-sided, first-order approximation for the surface vorticity is used since it is stable compared to second-order schemes. The singular point ($r = 1, z = 1$) is locally limited and does not appear in the finite-difference algorithm (Lugt & Haussling 1973). The boundary condition for the temperature at the insulated sidewall is $\vartheta^n_{i,m} = \vartheta^n_{i,m-1}$, where the subscripts i and j denote the ith and jth points in the z- and r-directions respectively. $j = m$ is the wall point with n the time step.

The integration process is carried out in the following sequence. The new time level for the vorticity $\zeta^{n+1}_{i,j}$, the velocity component $v^{n+1}_{i,j}$, and the temperature $\vartheta^{n+1}_{i,j}$ is computed at the inner points of the container. The stream function $\psi^{n+1}_{i,j}$ is subsequently computed from (14). The last step of the cycle concludes with the calculation of the unknown values of the vorticity and the temperature at the corresponding boundaries of the domain. The computations are started from the state at rest and are performed until the steady state is reached, which is approximately attained when

$$\sum_{i,j} |\psi^n_{i,j} - \psi^{n-1}_{i,j}| < 10^{-4}. \tag{17}$$

This 'almost steady state' is designated t_F.

The computer program was checked with various grid sizes. Most of the computations were performed with a network of 51×51, but a few cases required 81×81 points because the bubble region needed higher accuracy. The program was further checked with results from Bertelà's (1979) computations, in particular for the temperature field. The verification with experiments is discussed in the next section.

For the values of the lines of constant ψ, v, and ϑ equal intervals were chosen. The set of streamlines was split into two parts:

$$\Delta\psi = c_1 \quad \text{for } \psi_{\min} \leqslant \psi \leqslant 0 \quad \text{outside the bubbles,}$$

$$\Delta\psi = c_2 \quad \text{for } 0 \leqslant \psi \leqslant \psi_{\max} \quad \text{inside the bubbles,}$$

with the constants $|c_1| \gg c_2$. In the figures plotted here, the z'-component was made dimensionless by $z' = z^*R$ so that the (r, z^*)-field was not distorted.

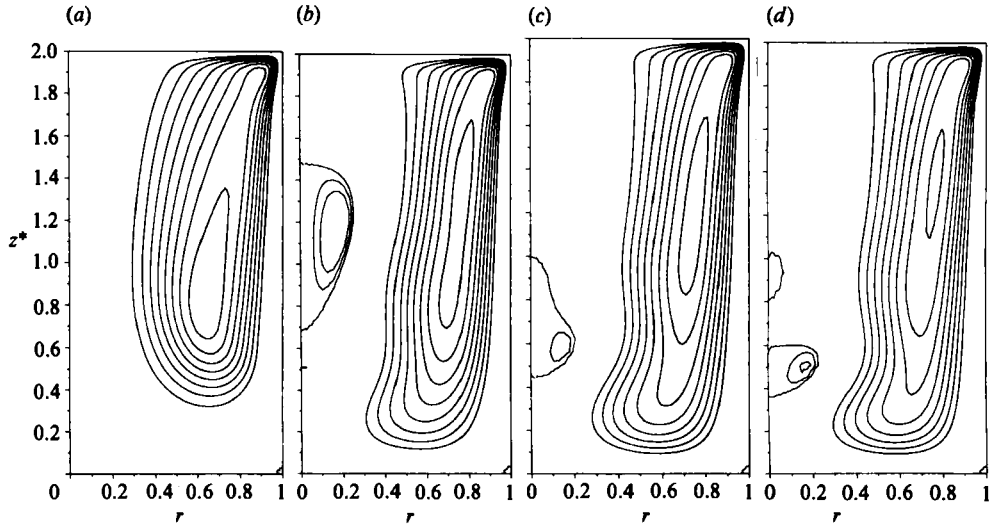

FIGURE 3. Lines of constant ψ for $Re = 2000$, $\delta = 2$ at four different times after the abrupt start of rotation of the lid. (*a*) $t = 51$; (*b*) 122; (*c*) 190; (*d*) 332.

4. Results

The examples selected are divided into two sets. In the first set is is assumed that $Ra = 0$. This means that the fluid is incompressible and homogeneous and that (12)–(14) for the flow field are decoupled from the energy equation (15) in such a way that the flow field is independent of the heat exchange but not vice versa. Thus, for $Ra = 0$ only the parameters Re and δ need be considered for studying the flow field whereas all parameters are involved for the computation of the temperature field. The seemingly odd values of the Reynolds numbers were chosen to compare the numerical results with experimental data in the literature. The values of $Pr = 0.7$ and 7.1 are those for air and water.

The second set of examples consists of cases with $Ra > 0$. This means that the bottom temperature T_0' was selected to be higher than the temperature T_1' of the lid and of the fluid at $t = 0$. This situation represents an unstable fluid stratification since $\rho = \rho_0(1 + \alpha\vartheta')$. The Eckert number is then positive too. The parameters Pr, Ra, and Ec were varied for two cases of Re and δ.

4.1. *Flow fields for* $Ra = 0$

Since the development of the flow field with one separation bubble from the state at rest has been described by Lugt & Haussling (1982), it suffices here to discuss briefly the process for the flow field with two bubbles, including some general comments made necessary by recent statements in the literature on stability (Escudier 1984; Leibovich 1984). The case $Re = 2000$, $\delta = 2$ has been selected (figure 3).

When the motion abruptly starts at $t = 0$, the flow develops from the corner region $r = 1$, $z = 1$ where the flow singularity occurs. With time, mass and momentum are carried through the evolving Ekman layer along the lid's surface and the Stewartson layer along the sidewall. During this period the streamlines and lines of constant azimuthal velocity are first monotonic (figure 3*a*) and change then to undulating shapes. They may be labelled inertial waves (sometimes also called centrifugal waves). It is surprising that the simple geometry of the container permits such a complex flow as that indicated in figure 1. The reason for this complexity is that the

Navier–Stokes equations for an incompressible, rotating fluid can have hyperbolic behaviour; that is, the flow can sustain waves. The wavy motion may cause stagnation points on the axis of rotation associated with a closed stream surface, the 'bubble' (figure 3*b*). This phenomenon is called 'vortex breakdown' because it fulfills all the criteria of vortex breakdown, for instance those given by Faler & Leibovich (1977): '...the development of a stagnation point on the axis, followed by a region of reversed axial flow encapsulated by a greatly swollen stream surface'. The appearance of a stagnation point at the axis can easily be explained by the pressure increase caused by the diverging helical streamlines (see Batchelor's 1967, p. 546 inviscid flow solution) and has nothing to do with instability, a statement which was made recently also by Wedemeyer (1982). Escudier's limiting curves (which Escudier called 'stability boundaries') in figure 2 are thus transition curves in the sense of the appearance of stagnation points.

A second bubble is barely visible at $z^* = 0.52$ below the large one in figure 3*b*. The pulsating motion then shifts the large bubble down, decreasing its size, while the second bubble grows. The two bubbles coalesce to an oddly shaped single bubble of 'cucumber' shape (figure 3*c*). At this point it may be recalled that, in the transient phase of an abruptly started container flow, very large and oddly shaped separation bubbles can occur which at times occupy a great portion of the container and then vanish when $t \to \infty$ (Lugt & Haussling 1973). In the final, almost steady state at $t_F = 331$ two bubbles occur (figure 3*d*). Both clearly consist of one vortex ring or cell each, in contrast to the 'egg-shaped' bubble in swirling pipe flow which, according to Leibovich (1978), can have two cells. The bubbles in figure 3 can be of 'egg', 'onion', and 'cucumber' shapes. The 'onion' shape can even develop to a form with a concave top. The v-component never changes sign in the bubble in any of the cases studied (not shown in figure 3), in contrast to the results by Bossel (1973) and Randall & Leibovich (1973).

A comparison with swirling flows in pipes of straight or slightly increasing or abruptly enlarging walls (Narain 1977) suggests that the shape and occurrence of bubbles not only depend on the entrance and exit conditions of the streamtube under consideration (in addition to the flow parameters) but also on the geometry of the streamtube. When container flow is compared with swirling pipe flow, however, the following distinction must be made.

In experiments, axisymmetry is enforced in the container flow to a large degree in a natural way by the rotating lid and by recirculation. In contradistinction, the entrance and exit velocity profiles in the pipe flow might deviate from axisymmetry and the swirling flow in the pipe might be more prone to non-axisymmetric instabilities than the container flow (Escudier 1984; Leibovich 1984). In numerical calculations, on the other hand (for instance, by Grabowski & Berger 1976 for pipe flows) axisymmetry is enforced in both container and pipe flows throughout the whole flow domain. Thus, in these calculations there is no difference between the bubbles in a streamtube cut out of the container flow and those in a pipe except for the influence of the shape and the boundary conditions of the streamtube.

Steady-state solutions for various pairs of parameters Re and δ are shown in figures 4–11. In figure 4, δ is kept constant at $\delta = 2$ and Re is varied. This situation corresponds to following a vertical line in the diagram of figure 2. The case $Re = 1002$ lies outside the region in which vortex breakdown occurs (figure 4*a*). The streamlines in the lower part are monotonic, and no bubble exists. For $Re = 1492$ one bubble is visible, and for $Re = 1854$ two bubbles appear (figures 4*b*, *c*). The latter case may be compared with figure 3 (*d*) for $Re = 2000$ where the two bubbles are shifted downward,

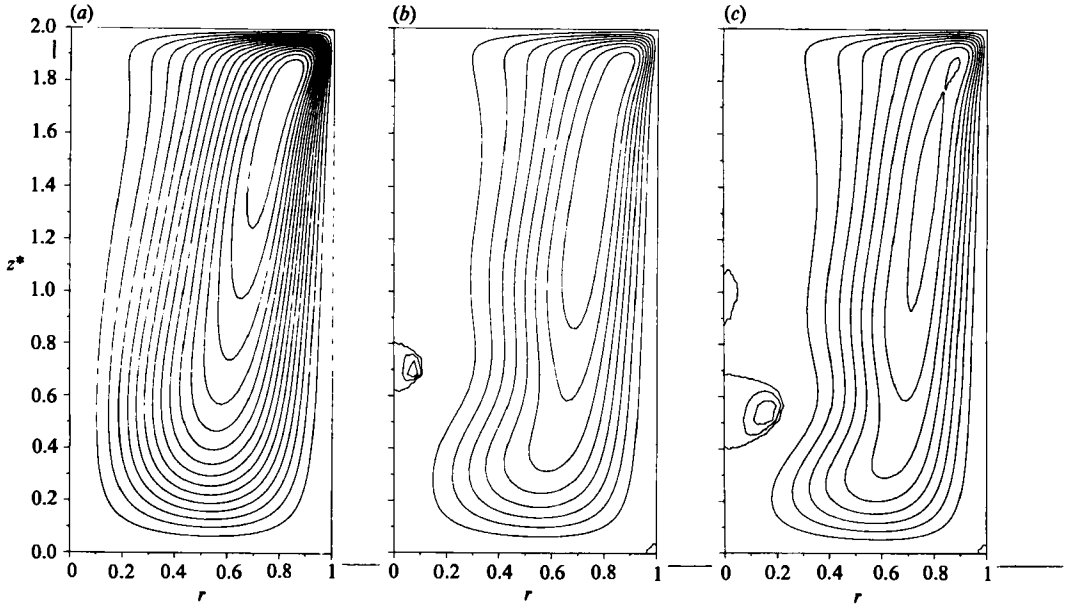

FIGURE 4. Lines of constant ψ at steady state for $\delta = 2$ and for (*a*) $Re = 1002$, (*b*) 1492, and (*c*) 1854.

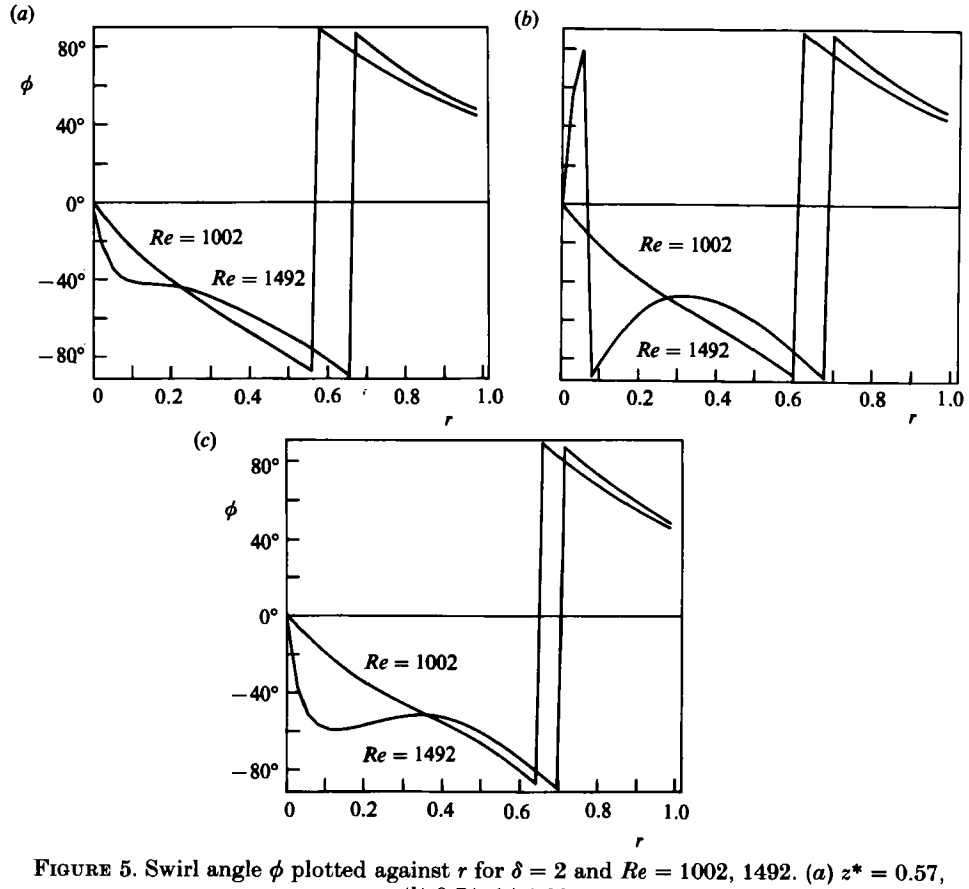

FIGURE 5. Swirl angle ϕ plotted against r for $\delta = 2$ and $Re = 1002$, 1492. (*a*) $z^* = 0.57$, (*b*) 0.74, (*c*) 1.00.

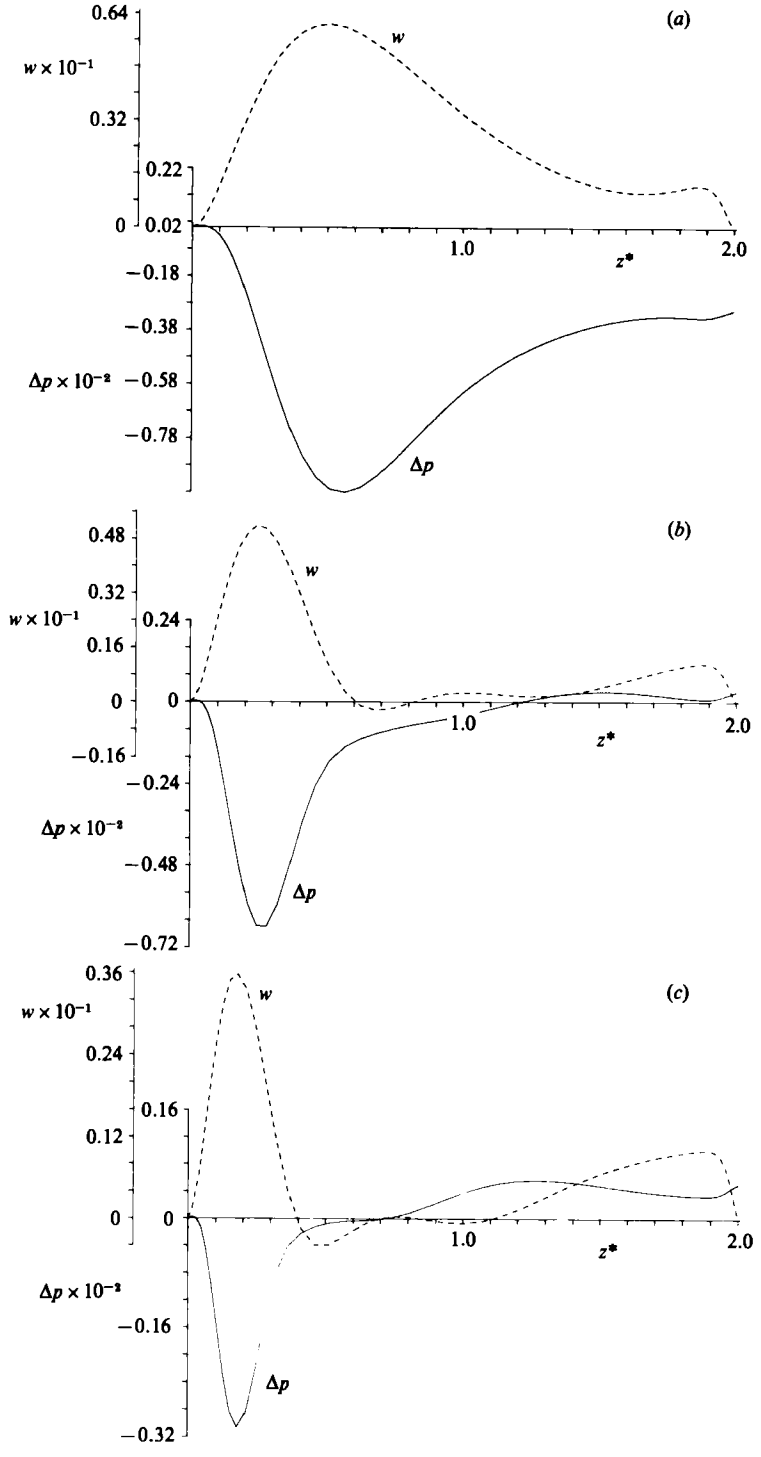

FIGURE 6. Δp and w along the axis $r = 0$ for $\delta = 2$ and for (*a*) $Re = 1002$, (*b*) 1492, (*c*) 1854. See the corresponding figure 4.

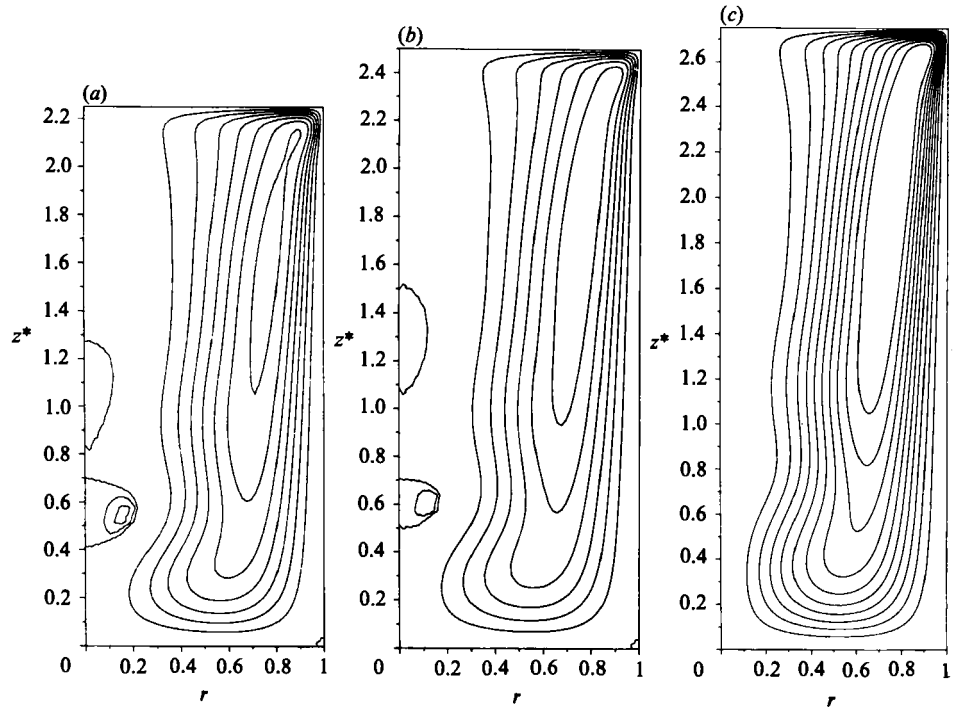

FIGURE 7. Lines of constant ψ at steady state for $Re = 2000$ and for (*a*) $\delta = 2.25$, (*b*) 2.5, (*c*) 2.75.

and a slight concavity of the top of the larger bubble is noticeable. For still larger Re the bubble vanishes.

A comparison of the streamlines in figure 4 reveals that the Stewartson layer at the sidewall barely changes from one case to another; no undulations are visible. The lower corner ($r = 1$, $z = 0$), however, initiates the wavy motion when the flow negotiates this corner and then is forced upward near the axis. The development of these waves depends on the Reynolds number. For low Reynolds numbers, of the order of 100, no waves occur because of the dominance of viscosity. When waves develop, their amplitudes increase with the Reynolds number and cause diverging streamlines around the axis from $z^* \approx 0.3$ and beyond. The meridional flow weakens near the axis whereas, simultaneously, the v-component close to the bottom and the axis strengthens (not shown in figure 4). It is this combination of weaker meridional flow and stronger rotation near the axis that increases the local swirl angle $\phi = \tan^{-1} v'/w'$, or to be more precise, steepens the inclination $\mathrm{d}\phi/\mathrm{d}r$. This is clearly displayed in figure 5 which also reveals the shift of the centre of the main circulation toward the sidewall with increasing Re. As a consequence of the diverging streamlines in the lower part of the container axis, the pressure rises along the axis much sooner (about $z^* = 0.3$) and steeper for $Re = 1492$ and 1854 than for $Re = 1002$ as can be seen in figure 6 in which Δp is computed from

$$(\Delta p)_{r=0} = \int_0^z \left[-w \frac{\partial w}{\partial z} + \frac{1}{Re} \left(2 \frac{\partial^2 w}{\partial r^2} + \frac{1}{\delta^2} \frac{\partial^2 w}{\partial z^2} \right) + \frac{Ra\,\vartheta}{\delta^2} \right] \delta^2 \,\mathrm{d}z. \tag{18}$$

The axial component w rises and then decreases along the axis. For $Re = 1492$ and 1854 w becomes zero and negative in a certain interval, signalling a stagnation point

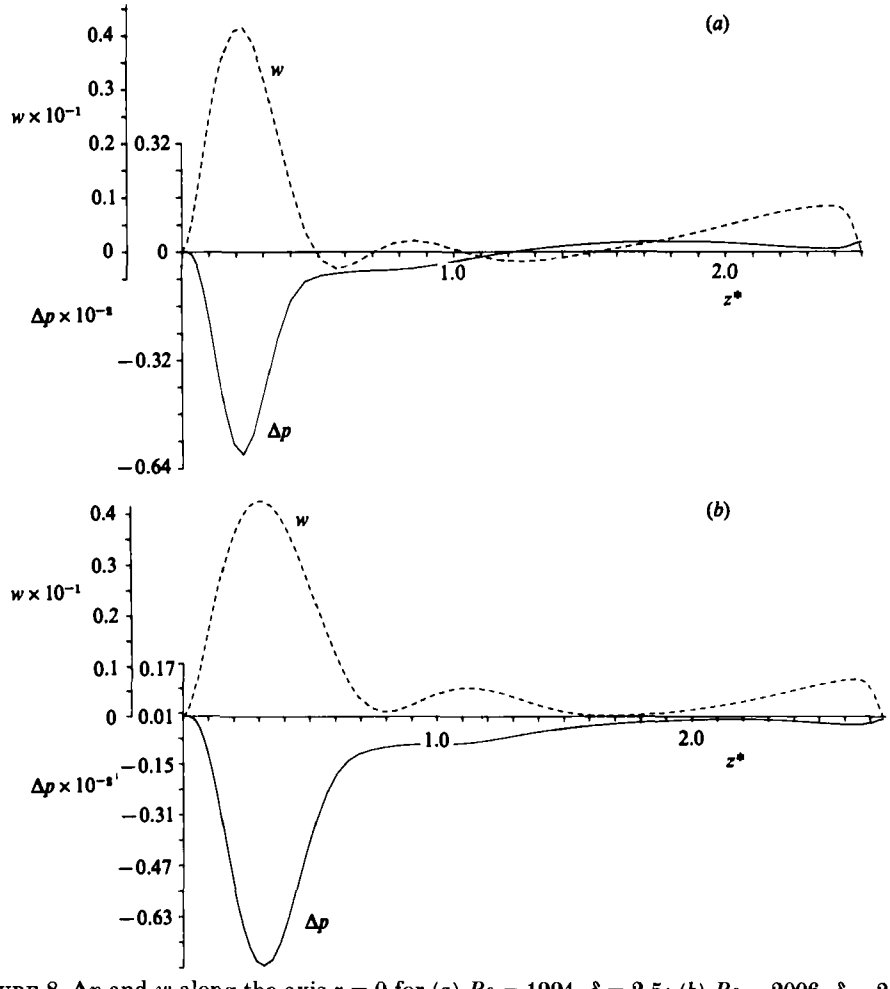

FIGURE 8. Δp and w along the axis $r = 0$ for (*a*) $Re = 1994$, $\delta = 2.5$; (*b*) $Re = 2006$, $\delta = 2.75$. See the corresponding figures 7 (*b*, *c*).

and the existence of a separation bubble. At $Re = 1854$ the wavyness is so strong that two bubbles appear. With further increase of Re the bubbles move upstream, a behaviour well-known from other studies of vortex breakdown (figure 3*d*). At still larger Re, as shown by an analysis not presented here, the w-component of the velocity strengthens slightly relative to the v-component in such a way that no bubble develops. This extremely subtle interplay is graphically demonstrated in the next paragraph for other cases.

In figure 7, Re is kept constant at approximately 2000, and δ is varied. This situation corresponds to following a horizontal line in figure 2, starting from $\delta = 2$ (figure 3*d*) over $\delta = 2.25$ and 2.5 to $\delta = 2.75$ (figures 7*a*, *b*, *c*). In the two extremes $\delta \ll 1$ and $\delta \gg 1$ no undulations occur. In the first case they have no chance to develop, since the corners are far away from the axis, and in the second case the undulations become longer and their amplitudes smaller because of the effects of the sidewalls in suppressing waves and increasing the influence of viscosity. In fact, increasing δ has an effect similar to decreasing Re. The two bubbles in figure 7 (*a*) move away from the bottom with increasing δ (figure 7*b*), the lower bubble becomes smaller,

and then, in figure 7(*c*), the bubbles have vanished for $\delta = 2.75$. Figure 8 gives information on the pressure and w-component along the axis. It is remarkable how similar these cases are and that small changes of the main circulation determines the appearance of the bubbles. As can be seen immediately, the flow field around the axis is very weak, at least from $z^* = 0.5$ on.

For $Re = 2752$, $\delta = 3.25$ (figure 9) an extremely long time is necessary to reach the almost steady state, and even then it is not certain whether changes might still occur in the axial region, which is very sensitive to small disturbances of the main circulation. At $t \approx 3500$ three bubbles appear, and at $t = 6405$ the upper two bubbles have coalesced to form a 'cucumber' with two cells, visible in the photograph of figure 9(*b*) but not in figure 9(*a*). The w-component is almost nil inside the 'cucumber'. The extreme time spans needed to reach a steady state are an indication that the border of unsteadiness is being approached and this is verified *a posteriori* by experiments (figure 2).

One attempt was made to compute the flow field in the turbulent range: $Re = 5450$, $\delta = 1.75$. The time history of ψ at an inner point shows chaotic behaviour (figure 10). It may be recalled, however, that the computed flow is forced to be axisymmetric and may not be realistic. Still, Escudier (1984) observed that 'Until well into the unsteady-flow domain, the flow shows negligible departure from axisymmetry'.

The numerical computations are compared with photographs and measurements published by Vogel (1968), Ronnenberg (1977), and Escudier (1984). The position h of the lower stagnation point of the bubbles measured in fractions of H, and the vertical size s of the bubbles are used for comparison (table 1).

The data of the numerical computations for h/H are smaller than those from Escudier's photographs, and the numerical data for s/H are in general larger. It may be mentioned that it is often difficult to determine h/H and s/H from the photographs and that the streaklines in the photographs do not always reflect the exact boundary of the bubble. Also photographs intentionally over-emphasize the bubble region although the fluid motion there is very weak in reality. Figure 11 shows good agreement between the photograph and numerical computations for $Re = 1854$ but less agreement for $Re = 2752$ in figure 9. In the latter case, which is located in figure 2 at the lower tip of the limiting curve for three bubbles and which borders on unsteadiness, tiny changes of the flow field after the long transient phase may still have a large effect on the location of those weak bubbles. Other than these discrepancies, the overall agreement is good, and the experiments confirm the assumption that axisymmetric solutions of the Navier–Stokes equations are stable.

4.2. *Temperature fields for* $Ra = 0$

For the particular case $Re = 1350$, $\delta = 1.58$ the Prandtl number was varied. Very small values of Pr mean dominance of heat diffusion over heat convection. Figure 12(*a*) with $Pr = 0.01$ reveals almost horizontal strata of isotherms, slightly bent down near the sidewall where the flow is strongest. The temperature at the axis drops almost linearly (figure 13). This situation changes drastically for $Pr = 0.7$ (figure 14*a*): convection turns the isotherms in the vertical direction, and the heat transfer near the bottom and the lid rises greatly. This effect is even more pronounced with increasing Pr (figures 14*b–d*). The corresponding Nusselt numbers, defined by $Nu = -\partial\vartheta/\partial z$, are plotted against r for the bottom and the lid in figure 15. For $Pr = 0.01$ (figure 15*a*) the heat transfer is quite evenly distributed over the bottom and the lid. With increasing Pr the bulk of the heat transfer concentrates at the centre

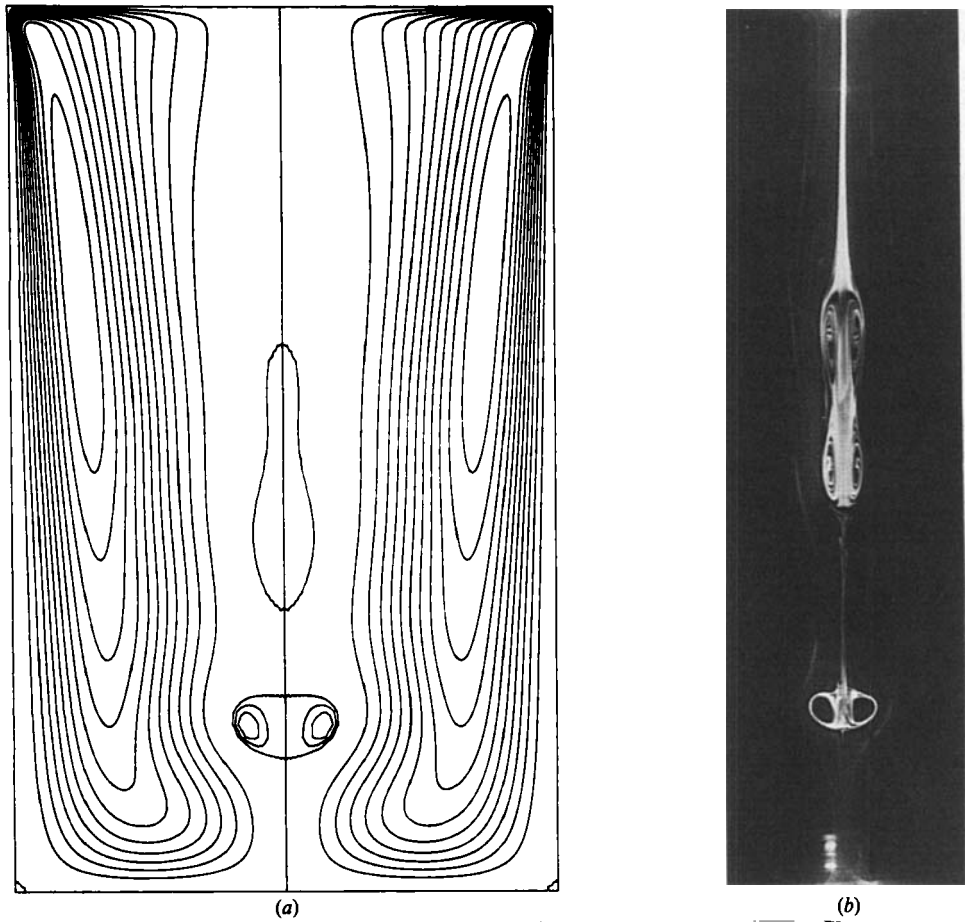

FIGURE 9. Lines of constant ψ in the total meridional plane for $Re = 2752$ and $\delta = 3.25$ at steady state. (*a*) Numerical computation and (*b*) photographs of the axis region by M. P. Escudier.

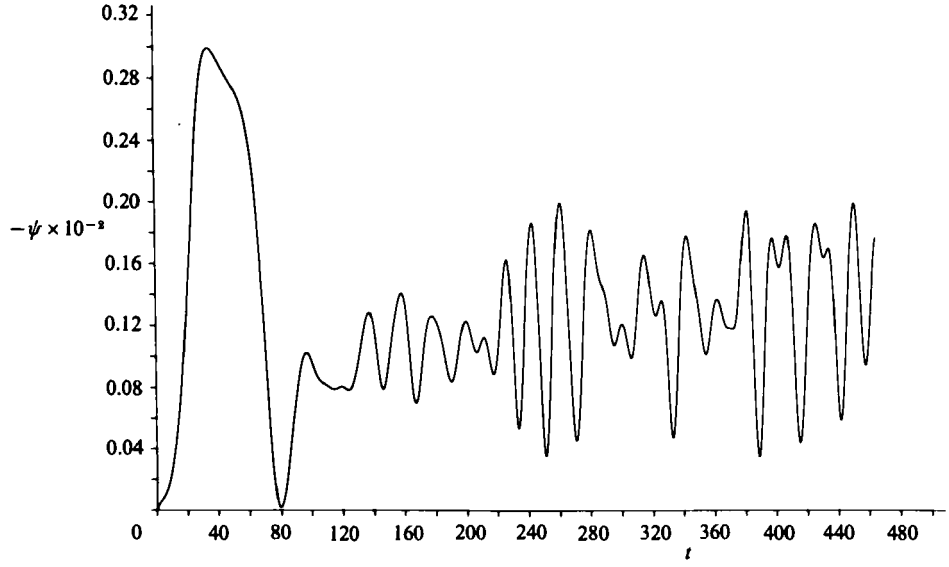

FIGURE 10. Time history of ψ at a point near the centre of flow circulation for $Re = 5450$ and $\delta = 1.75$.

			Experiment		Numerical computations	
Re	δ	Source of experiment	h/H	s/H	h/H	s/H
1130	1.58	Vogel	0.45	0.03	0.45	0.04
1350	1.58	Ronnenberg	0.30	0.14	0.31	0.14
1492	2	Escudier	0.34	0.06	0.31	0.09
1580	1.59	Ronnenberg	0.24	0.14	0.25	0.12
1854	2	Escudier				
		Bubble 1	0.21	0.16	0.20	0.14
		Bubble 2	0.52	?	0.44	
1994	2.5	Escudier				
		Bubble 1	0.24	0.06	0.20	0.08
		Bubble 2	0.54	0.08	0.43	0.17
2752	3.25	Escudier				
		Bubble 1	0.18	~ 0.04	0.15	0.07
		Bubble 2	0.43	~ 0.25	0.32	0.30

TABLE 1. Comparison of the numerical results with experiments including photographs of Vogel (1968), Ronnenberg (1977) and Escudier (1984)

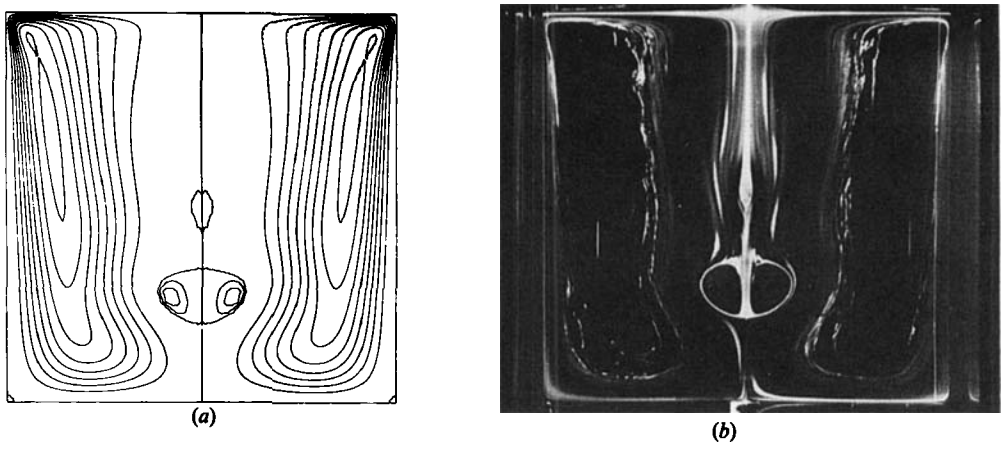

FIGURE 11. Lines of constant ψ in the total meridional plane for $Re = 1854$ and $\delta = 2$. (*a*) Numerical computation and (*b*) photograph by M. P. Escudier.

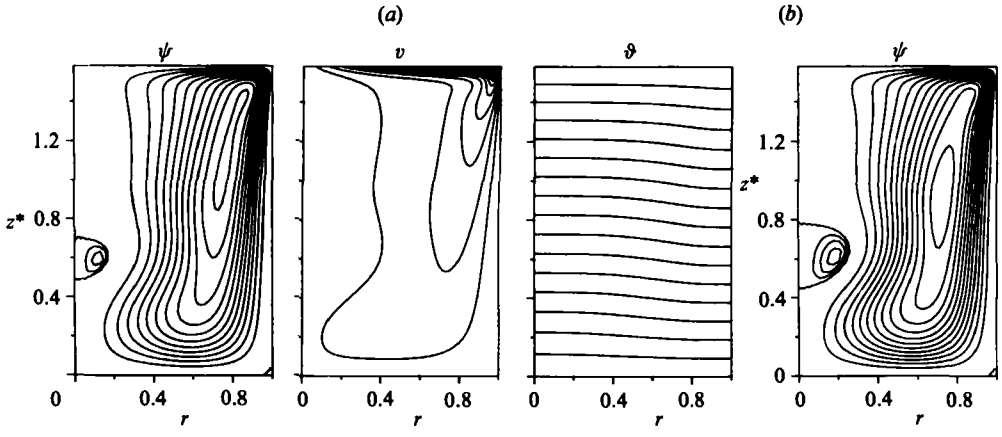

FIGURE 12. (*a*) Lines of constant ψ, v, and ϑ for $Re = 1350$, $\delta = 1.58$, $Ec = 0.01$, $Pr = 0.01$, and $Ra < 0.01$ at steady state, and (*b*) lines of constant ψ for the same parameters but with $Ra = 0.2$.

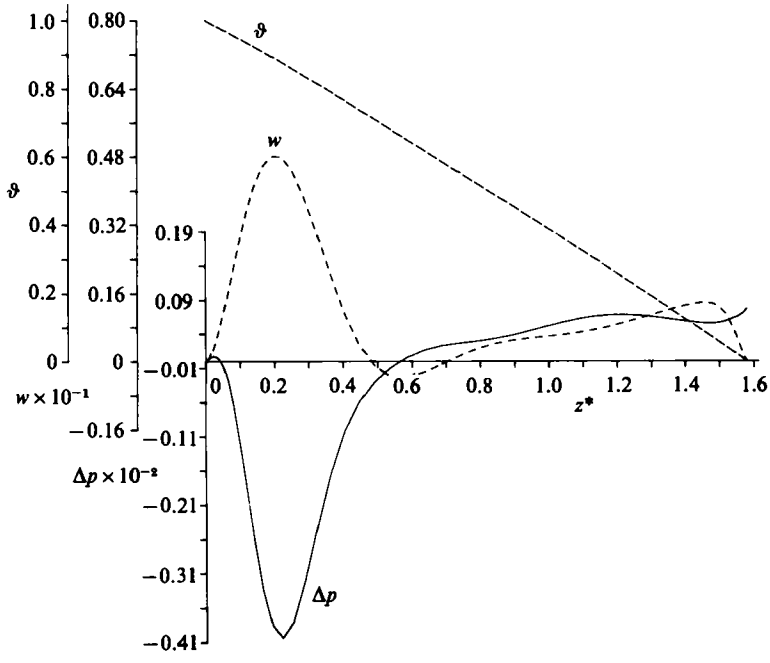

FIGURE 13. Δp, w, and ϑ along the axis $r = 0$ for the case of figure 12(*a*).

of the lid and near the outer part of the bottom (figures 15*b–d*). This behaviour is because heat transfer is determined more and more by heat convection with increasing Pr. If this heat convection is directed away from the solid surface, and heat transfer becomes smaller than if it is directed toward the surface. Near the axis in figures 14(*b, c, d*) there is a warm, mushroom-like core close to T_0' that narrows with increasing Pr. The top of the mushroom is caused by the bubble. However, according to the existence of a maximum principle that ϑ cannot have a local extremum inside the fluid, a temperature bubble cannot occur as long as $Ec = 0$ (Lugt 1985). In figure 14(*d*), with $Ec = 0.01$, a weak temperature bubble does exist.

For $Pr = 0.01$, $Ra = 0$, a change in the Eckert number from 0 to 1.0 has no visible effect on the temperature field.

4.3. *Flow fields with temperature effects* ($Ra > 0$)

The term with Ra in (12) connects the Navier–Stokes equations with the energy equation. The first series of computations determined the Ra at which this connection becomes effective. For $Re = 1350$, $\delta = 1.58$, $Pr = 0.01$, $Ec = 0.01$ no influence was observed when $Ra \leqslant 0.01$. With increasing Ra the bubble becomes larger (figure 12*b*). The heavier fluid at the top rushes down along the sidewall and causes near the axis a wave larger than that of the fluid without the gravitational pull. No steady state was obtained for $Ra = 0.3$, rather a periodic oscillation of the flow field was observed (figure 16). The temperature field remained almost steady.

The Rayleigh number Ra introduced in this paper in (9) is related to $Ra^* = \alpha\rho_0 c_p g(T_0' - T_1') H^3/\nu\lambda$ used in the literature for purely natural convection by

$$Ra^* = Re^2 Pr\, \delta^2 Ra. \tag{19}$$

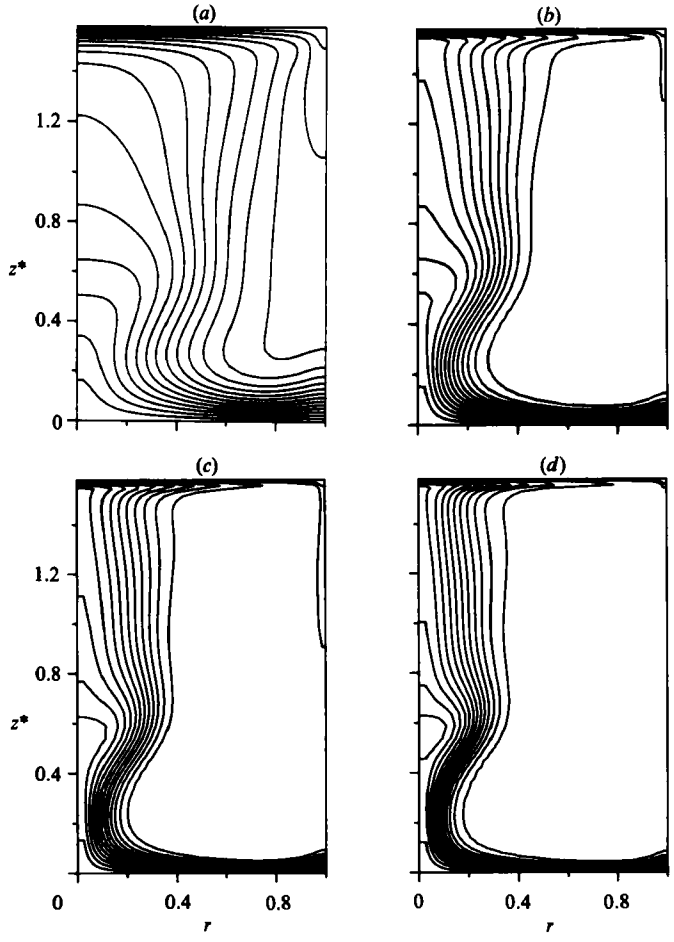

FIGURE 14. Lines of constant ϑ (isotherms) for $Re = 1350$, $\delta = 1.58$, and for (*a*) $Pr = 0.7$, (*b*) 7.1, (*c*) 15, (*d*) 30.

For instance, $Re = 1350$, $\delta = 1.58$, $Ra = 0.05$, $Pr = 0.01$ and 10, corresponds to $Ra^* = 2275$ and $Ra^* = 2.275 \times 10^6$ respectively.

In the second series of computations the Prandtl number was varied from $Pr = 0.01$–10 for $Ra = 0.01$, $Re = 1854$, $\delta = 2$, $Ec = 0.01$. Again, for $Pr = 0.01$ no difference was noticed with the case $Ra = 0$ (figure 4*c*). However, with increasing Pr the axis region including the bubbles becomes very sensitive to tiny changes in the main circulation. For $Pr = 2$ only one bubble is left from the original two (figure 17*a*), and for $Pr = 10$ no bubble occurs (figure 17*b*).

In the last series of computations the Eckert number was varied from 0.1 to 4 (figure 18). The constant parameters are $Re = 1350$, $\delta = 1.58$, $Ra = 0.05$, and $Pr = 0.7$. In these cases dissipation generates heat where large velocity gradients exist, and dissipation can influence both flow and temperature fields considerably. The temperature inside the fluid can exceed $\vartheta = 1$ and can exhibit a local maximum (Lugt 1985). The ϑ-curves for $Ec = 0.1$ in figure 18(*a*) do not yet display such a maximum but reach values up to 1.01 at the axis of rotation close to the corner $z^* = 0$, $r = 0$. For $Ec = 4$ (figure 18*b*) two maxima of ϑ occur at the axis: in a small region below the bubble with $\vartheta_{\max} = 1.026$, and in the bubble itself with

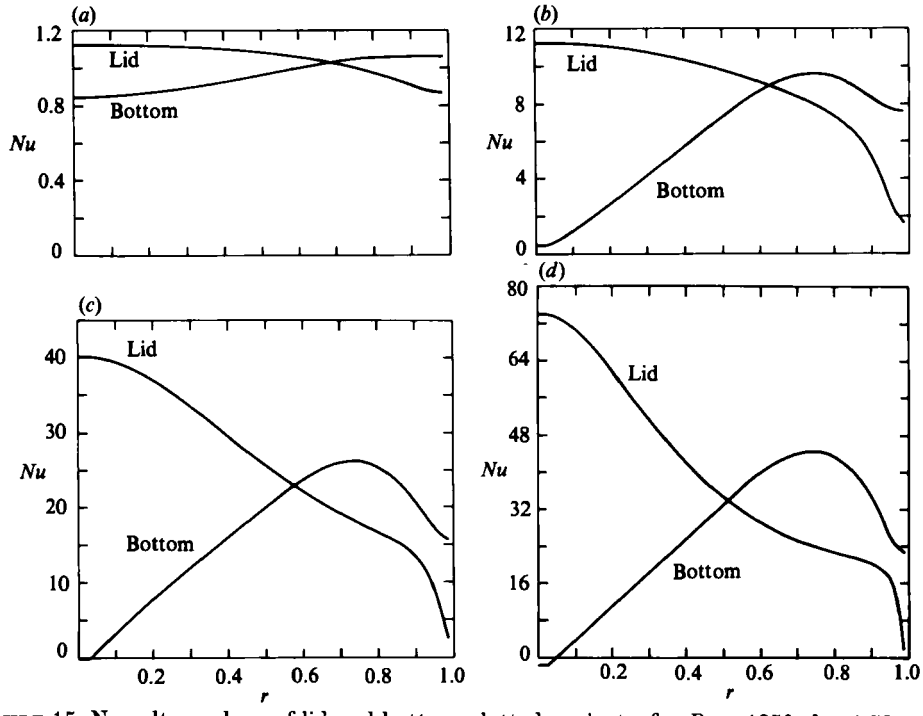

FIGURE 15. Nusselt numbers of lid and bottom plotted against r for $Re = 1350$, $\delta = 1.58$, and for (*a*) $Pr = 0.01$, (*b*) 0.7, (*c*) 7.1, (*d*) 30.

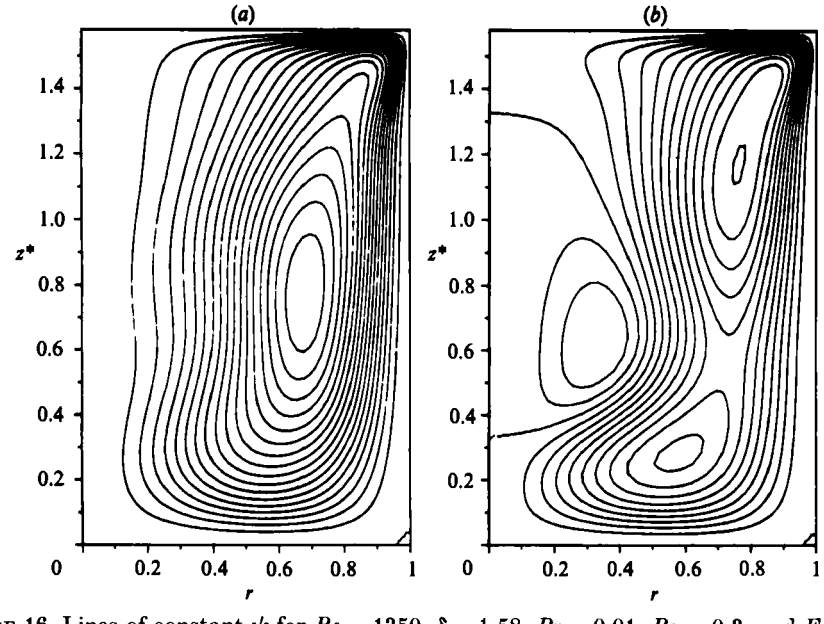

FIGURE 16. Lines of constant ψ for $Re = 1350$, $\delta = 1.58$, $Pr = 0.01$, $Ra = 0.3$, and $Ec = 0.01$ at times of (*a*) minimum and (*b*) maximum of the amplitude.

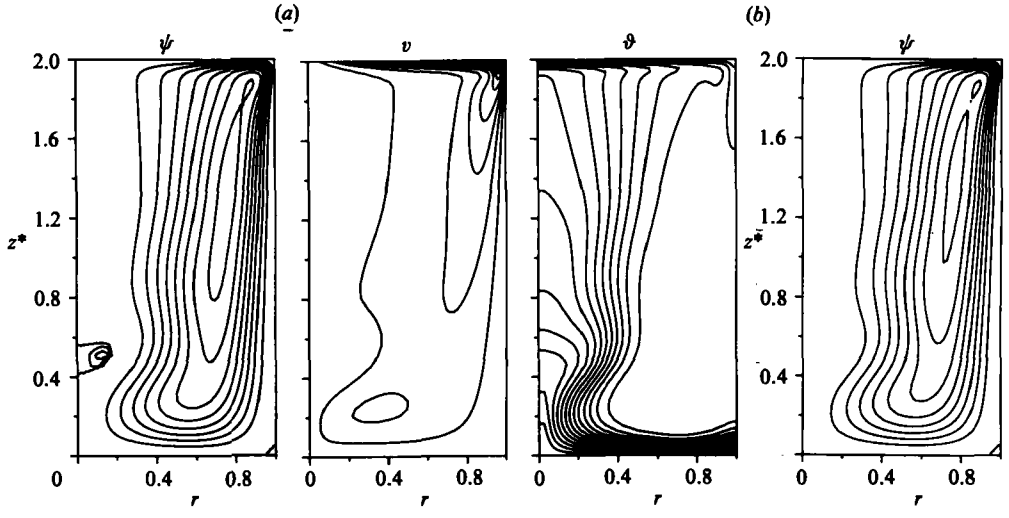

FIGURE 17. (*a*) Lines of constant ψ, v, and ϑ for $Re = 1854$, $\delta = 2$, $Pr = 2$, $Ra = 0.01$, and $Ec = 0.01$ at steady state, and (*b*) lines of constant ψ for the same parameters but with $Pr = 10$.

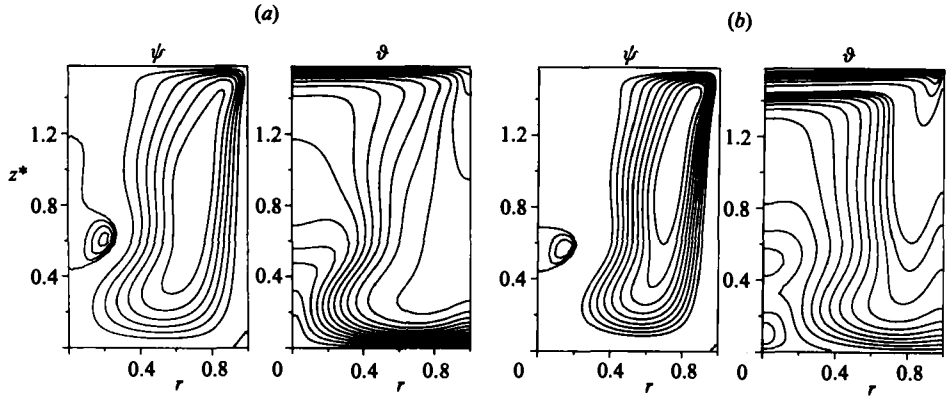

FIGURE 18. Lines of constant ψ and ϑ for $Re = 1350$, $\delta = 1.58$, $Pr = 0.7$, $Ra = 0.05$, and for (*a*) $Ec = 0.1$, (*b*) 4 at steady state.

$\vartheta_{max} = 1.015$. These local maxima are also visible in figure 19(*b*) which may be compared with figure 19(*a*) for $Ec = 0.1$. Figure 19, moreover, displays a large increase of the pressure along the axis. Finally, the local Nusselt numbers for the lid and the bottom in figure 20 indicate that for $Ec > 0$ the total heat flux on the lid is larger than on the bottom owing to the generation of heat inside the fluid. This is dramatically illustrated in figure 20(*b*), which shows that the heat flux on the bottom is almost nil for $Ec = 4$.

5. Conclusions

The simple geometry of the container with a rotating lid can cause complex flow patterns since rotating incompressible homogeneous and Boussinesq fluids can sustain waves. The occurrence of separation bubbles in steady waves, visible as

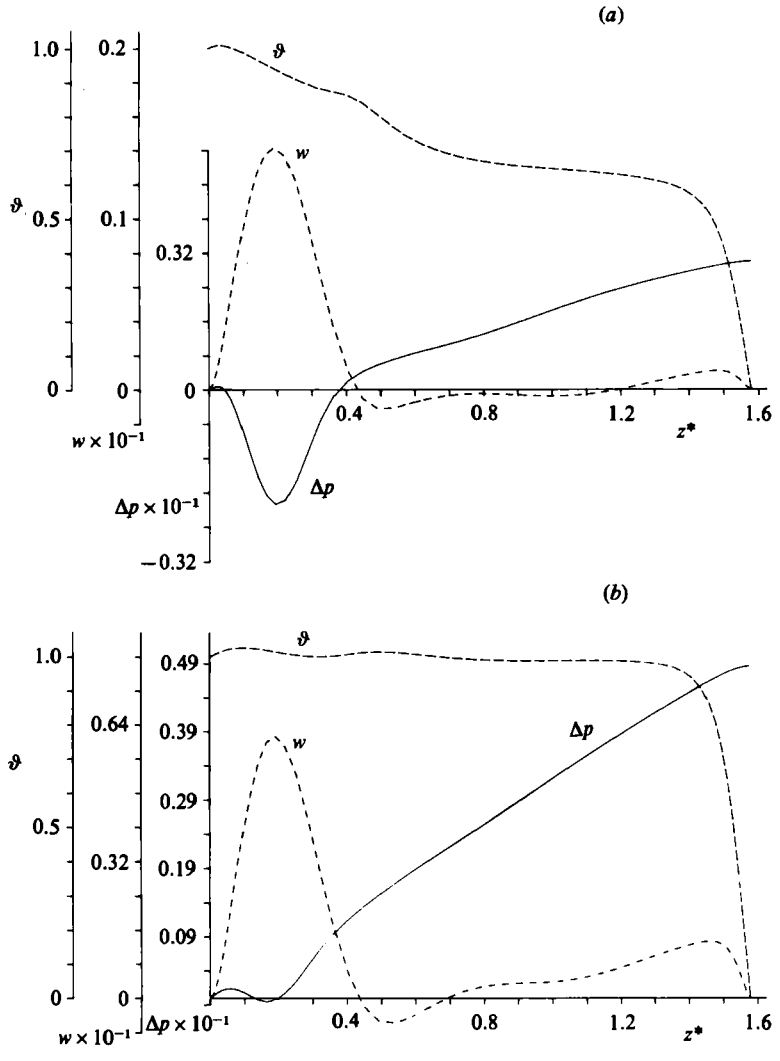

FIGURE 19. Δp, w, and ϑ and the axis $r = 0$ for the two cases of figure 18: (*a*) $Ec = 0.1$, (*b*) 4.

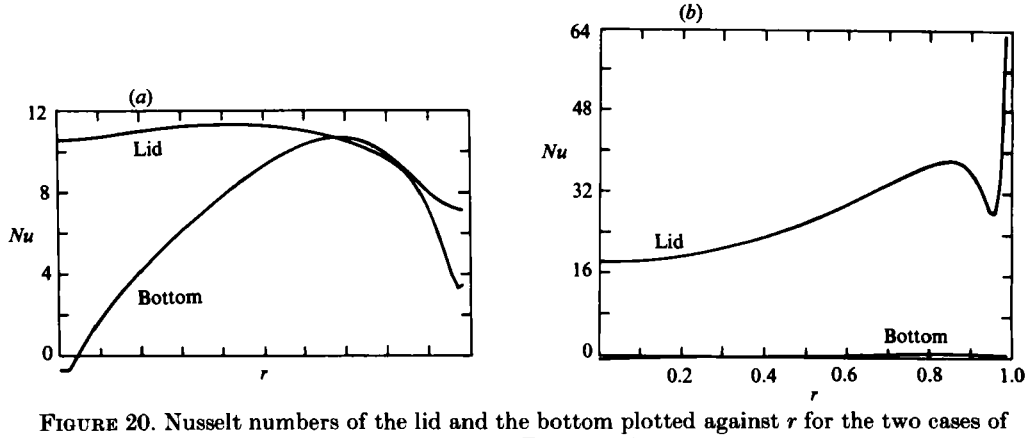

FIGURE 20. Nusselt numbers of the lid and the bottom plotted against r for the two cases of figure 18: (*a*) $Ec = 0.1$, (*b*) 4.

undulatory streamlines in the meridional plane, is due to the adverse pressure gradient in diverging helical flows causing the occurrence of stagnation points. Instability plays no part in this phenomenon, which can be interpreted as axisymmetric vortex breakdown according to the commonly accepted definition.

The extremely weak flow in the axial region where bubbles occur is very sensitive to small changes in the main circulation. The bubbles have essentially three types of contours: 'egg', 'onion', and 'cucumber' shapes, and only in the latter type were two cells observed in photographs.

For $\delta \ll 1$ and $\delta \gg 1$ no bubbles occur. In between, depending on the parameters involved, one, two, and three bubbles can exist simultaneously, as depicted in figure 2 for $Ra = 0$.

The temperature field plays no part in the occurrence of bubbles for $Ra = 0$, since the energy equation is decoupled from the Navier–Stokes equations. For $Ra > 0$ ($Ra < 0$ is not considered in this paper) the occurrence and properties of the bubble depend on the interplay between the undulatory streamlines in the meridional plane and the azimuthal velocity component. This interplay, which determines the upstream swirl angle, is a function of Re, Ra, Pr, and Ec.

The authors would like to thank Dr M. P. Escudier, Brown Boveri Research Center, for providing the photographs in figures 9 and 11.

REFERENCES

BATCHELOR, G. K. 1967 *An Introduction to Fluid Dynamics.* Cambridge University Press.

BERTELÀ, M. 1979 A non-isothermal fluid rotating in a finite cylindrical container. *Proc. 1st Intl Conf. on Numerical Methods in Thermal Problems* (ed. R. W. Lewis & K. Morgan), p. 279.

BERTELÀ, M. & GORI, F. 1982 Laminar flow in cylindrical container with a rotating cover. *Trans ASME* I: *J. Fluids Engng* **104**, 31.

BOSSEL, H. H. 1973 Swirling flows in streamtubes of variable cross section. *AIAA J.* **11**, 1161.

BRETHERTON, F. P., CARRIER, G. F. & LONGUET-HIGGINS, M. S. 1966 Report on the I.U.T.A.M. symposium on rotating fluid systems. *J. Fluid Mech.* **26**, 393.

DORFMAN, L. A. & ROMANENKO, Y. B. 1966 Flow of viscous fluid in a cylindrical vessel with a rotating cover. *Izv. Acad. Nauk. SSSR, Mek. Zhid. i Gaza* **1**, 63.

ESCUDIER, M. P. 1984 Observations of the flow produced in a cylindrical container by a rotating endwall. *Exp. Fluids* **2**, 189.

ESCUDIER, M. P. & ZEHNDER, N. 1982 Vortex-flow regimes. *J. Fluid Mech.* **115**, 105.

FALER, J. H. & LEIBOVICH, S. 1977 Disrupted states of vortex flows and vortex breakdown. *Phys. Fluids* **20**, 1385.

GRABOWSKI, W. J. & BERGER, S. A. 1976 Solutions of the Navier–Stokes equations for vortex breakdown. *J. Fluid Mech.* **75**, 525.

GRAY, D. D. & GIORGINI, A. 1976 The validity of the Boussinesq approximation for liquids and gases. *Intl J. Heat Mass Transfer* **19**, 545.

GROHNE, D. 1956 Über die laminare Strömung in einer kreiszylindrischen Dose mit rotierendem Deckel. *Nachr. Akad. Wiss. Göttingen, Math.-Phys.* Kl IIa (Nr. 1), 263.

LEIBOVICH, S. 1978 The structure of vortex breakdown. *Ann. Rev. Fluid Mech.* **10**, 221.

LEIBOVICH, S. 1984 Vortex stability and breakdown: survey and extension. *AIAA J.* **22**, 1192.

LUGT, H. J. 1985 Vortex flow and maximum principles. *Am. J. Phys.* **53**, 649.

LUGT, H. J. & HAUSSLING, H. J. 1971 Transient Ekman and Stewartson layers in a rotating tank with a spinning cover. *IUTAM Symp. on Unsteady Boundary Layers.* p. 1366. Quebec: Laval University Press.

LUGT, H. J. & HAUSSLING, H. J. 1973 Development of flow circulation in a rotating tank. *Acta Mech.* **18**, 255.

LUGT, H. J. & HAUSSLING, H. J. 1982 Axisymmetric vortex breakdown in rotating fluid within a container. *Trans. ASME* E: *J. Appl. Mech.* **49**, 921.

MAXWORTHY, T. 1972 On the structure of concentrated, columnar vortices. *Astron. Acta* **17**, 363.

NARAIN, J. P. 1977 Numerical prediction of confined swirling jets. *Computers and Fluids* **5**, 115.

PAO, H. P. 1970 A numerical computation of a confined rotating flow. *Trans. ASME* E: *J. Appl. Mech.* **37**, 480.

PAO, H. P. 1972 Numerical solution of the Navier–Stokes equations for flows in the disk–cylinder system. *Phys. Fluids* **15**, 4.

RANDALL, J. D. & LEIBOVICH, S. 1973 The critical state: a trapped wave model of vortex breakdown. *J. Fluid Mech.* **58**, 495.

RONNENBERG, B. 1977 Ein selbstjustierendes 3-Komponenten-Laserdoppleranemometer nach dem Vergleichsstrahlverfahren, angewandt für Untersuchungen in einer stationären zylindersymmetrischen Drehströmung mit einem Rückstromgebiet. *Max-Planck-Institut für Strömungsforschung, Göttingen, Bericht* 20.

SARPKAYA, T. 1971 Vortex breakdown in swirling conical flows. *AIAA J.* **9**, 1792.

SCHMIEDEN, C. 1928 Über den Widerstand einer in einer Flüssigkeit rotierenden Scheibe. *Z. Angew. Math. Mech.* **8**, 460.

VETTIN, F. 1857 Meteorologische Untersuchungen. *Poggendorfs Ann. der Physik.* **102**, 246.

VOGEL, H. U. 1968 Experimentelle Ergebnisse über die laminare Strömung in einem zylindrischen Gehäuse mit darin rotierender Scheibe. *Max-Planck-Institut für Strömungsforschung, Göttingen, Bericht* 6.

WEDERMEYER, E. 1982 Vortex Breakdown. *AGARD-VKI Lecture Series*, vol. 121, 9-1.

WEGENER, A. 1917 *Wind- und Wasserhosen in Europa.* Braunschweig: Vieweg.